Loss of PAX6 alters the excitatory/inhibitory neuronal ratio in human cerebral organoids.

Wai Kit Chan[1], Danilo Negro[1], Victoria M Munro[1], Helen Marshall[1], Zrinko Kozić[1], Megan Brown[1], Mariana Beltran[2], Neil C Henderson[2], David J Price[1], John O Mason[1]

[1]Simons Initiative for the Developing Brain, Centre for Discovery Brain Sciences, University of Edinburgh, Hugh Robson Building, George Square, Edinburgh EH8 9XD, UK

[2]Institute for Regeneration & Repair (IRR), University of Edinburgh, Edinburgh Bioquarter, 4 – 7 Little France Drive, Edinburgh EH16 4UU, United Kingdom.

Corresponding Author email address: waikit.chan@ed.ac.uk

Keywords: PAX6, human cerebral organoid, neurodevelopment, cell fate, interneurons, cerebral cortex

Summary Statement (30 words)

To identify likely roles of PAX6 during human embryonic development, we generated and analysed human PAX6 mutant cerebral organoids, revealing strong similarities and some differences to Pax6's well-known roles in rodents.

Abstract (180 words)

The transcription factor PAX6 is a crucial regulator of multiple aspects of embryonic forebrain development. Its well-known roles in mice include regulating differentiation of excitatory and inhibitory neurons in the embryonic cortex. PAX6's roles during human forebrain development are less well understood. Using human cerebral organoids, we investigated PAX6's roles in human neurodevelopment. Homozygous PAX6 mutant (*PAX6*$^{-/-}$) organoids were larger than controls and contained inhibitory cell types not found in *PAX6*$^{+/+}$ controls. These inhibitory cells exhibited clear transcriptomic similarities and comparable distribution to analogous inhibitory cells previously described in *Pax6*$^{-/-}$ mice. Differentiation trajectory inferencing showed that the inhibitory cells were generated from both radial glia and neuroectodermal progenitor populations. Inferring cell-cell communication using CellChat showed that loss of PAX6 in cerebral organoids increased the probability of cells engaging with inappropriate signalling pathways. Our findings indicate that while PAX6's role in controlling excitatory versus inhibitory neural differentiation is conserved, there are alterations in the activities of intercellular signalling pathways in human *PAX6*$^{-/-}$ cortical progenitors that have not been described in mice, indicating potential species-specific mechanistic differences.

Introduction

Neurons in the cerebral cortex fall into two major classes - excitatory and inhibitory (Cadwell et al., 2019). Imbalances between these two cell types are thought to underlie a variety of neurodevelopmental disorders (Bruining et al., 2020). The transcription factor PAX6 is a key regulator of embryonic forebrain development (Manuel et al., 2015; Ochi et al., 2022; Walcher et al., 2013). In mice, Pax6 is selectively expressed within the ventricular zone (VZ) of the dorsal telencephalon (Walther and Gruss, 1991), restricting GABAergic differentiation to the ganglionic eminences (Scardigli et al., 2003; Toresson et al., 2000). Accordingly, the pallium of *Pax6*$^{-/-}$ mice is significantly ventralised, with cortical progenitors generating ectopic inhibitory interneurons at the expense of glutamatergic differentiation (Holm et al., 2007; Kroll and O'Leary, 2005; Manuel et al., 2015). Our present understanding of human PAX6 is limited. PAX6 is expressed in VZ of the human telencephalon and diencephalon (Terzić and Saraga-Babić, 1999) and is expressed during neural induction in human cells *in vitro* (Zhang et al., 2010). Homozygous PAX6 mutations are either lethal or result in major brain defects including corpus callosum agenesis, cortical thinning, microcephaly, large midline cavities and hypoplastic brainstem (Glaser et al., 1994; Schmidt-Sidor et al., 2009; Solomon et al., 2009). Heterozygous PAX6 mutations show milder phenotypes including anterior commissure defects and regionalised cortical thinning (Bamiou et al., 2007; Sisodiya et al., 2001; Thompson et al., 2004; Yogarajah et al., 2016).

Given the challenges of studying human neurodevelopment directly, we turned to cerebral organoids, a human model system amenable to experimentation (Lancaster et al., 2013) to investigate the role of PAX6. We generated *PAX6*$^{-/-}$ induced pluripotent stem cells (iPSCs), differentiated them into cerebral organoids and found that PAX6 loss resulted in larger organoids containing novel cell types, primarily inhibitory neurons and progenitors. These findings align with previous observations in mice, indicating conservation across species in terms of PAX6's effect on excitatory neuronal development. We also found evidence that some signalling pathways not previously found to be affected in Pax6 mutant mice are altered in PAX6 mutant human cortical organoids. Our study provides new insights into PAX6's functions in human neurodevelopment and highlights the potential of cerebral organoids as tools to investigate gene function in human forebrain development.

76 **Results and discussion**

77

78 ***Generation of PAX6$^{-/-}$ iPSCs and organoids***

79 We derived *PAX6$^{-/-}$* mutant iPSC lines from the parental line NAS2 (Devine et al., 2011) using
80 CRISPR-Cas9 to insert a T residue into the paired box region of PAX6 (Fig 1A), causing a
81 frameshift mutation and resulting in premature termination of PAX6 protein at amino acid
82 residue 31, 20 residues downstream of the mutation. Paired box mutations have been
83 implicated in the brain malformations described in human patients (Tzoulaki et al., 2005) and
84 the paired domain alone is necessary and sufficient to regulate telencephalic development in
85 mice (Haubst et al., 2004). Two independent *PAX6$^{-/-}$* clones (A10 and B2) homozygous for this
86 mutation and two isogenic control clones were selected for further analysis. In both mutant
87 clones, no CRISPR off-target effects were detected via whole genome sequencing analysis of
88 the five predicted most likely sites. All lines expressed pluripotency markers NANOG, OCT3/4
89 and TRA-1-60 (Supp Fig 1A)(Devine et al., 2011). Organoids were grown from *PAX6$^{+/+}$* (control)
90 and mutant cell lines using a version of the Lancaster protocol (Lancaster et al., 2013) modified
91 by the inclusion of dual SMAD inhibition (Chambers et al., 2009) and growth factors BDNF &
92 NT3 (Birey et al., 2017)(Supp Fig 1B). Immunostaining for PAX6 confirmed absence of
93 functional PAX6 protein in mutant organoids (Fig 1C).

94

95 ***iPSC lines produce highly consistent organoids***

96 To assess the consistency of our differentiation protocol, day 60 organoids grown from both
97 *PAX6$^{-/-}$* mutant and two isogenic control lines were cryosectioned and stained for SOX2 (to
98 mark progenitors) and N-CAD (to identify neuroepithelium) (Fig 1D,E). Staining patterns were
99 highly consistent between organoids of the same genotype, but *PAX6$^{-/-}$* organoids appeared
100 larger than controls and contained fewer rosettes (radial arrangement of columnar epithelial
101 cells with a central lumen resembling a cross-section of the developing neural tube). Organoid
102 size was approximated by measuring the area of the widest cross-section of each organoid.
103 The cross-sectional area of *PAX6$^{-/-}$* organoids was 18.09 $\pm$ 1.80 mm^2 compared to 11.55 $\pm$ 2.40
104 mm^2 in controls (Fig 1D-F). The proportion of organoid tissue containing neural rosettes
105 (demarcated by SOX2 and N-CAD staining (Gomes et al., 2020)) was 1.4% $\pm$ 0.29% in *PAX6$^{-/-}$*
106 organoids and 12.68% $\pm$ 1.57% in controls (Fig 1G). This decrease was due to a dramatically
107 lower density of rosettes in *PAX6$^{-/-}$* organoids (Fig 1H). While *PAX6$^{-/-}$* organoids contained fewer

108 neural rosettes overall, the size of individual rosettes did not differ significantly between *PAX6*$^{-/-}$
109 organoids and controls (Fig 1I-J).
110
111 ***Altered cell composition in PAX6*$^{-/-}$ *cerebral organoids.***
112 To determine the effects of PAX6 loss on organoid cell type composition, we performed single
113 cell RNA sequencing (scRNAseq) on four batches of organoids grown from each of the four
114 iPSC lines (two mutant and two control). Ambient RNA, dead cells and doublets were removed
115 and cells were clustered independently using the Leiden algorithm (Traag et al., 2019) and
116 visualised using uniform manifold approximation and projection (UMAP). Initial clustering
117 analysis to compare UMAPs of individual organoids revealed clear consistency between
118 batches and identified a small number of samples containing primarily non-neuronal cell types
119 which were omitted from further study (Supp Fig 2A, asterisks). 77,846 cells were retained for
120 downstream analysis. Following reclustering, identities were assigned to clusters using cell
121 type specific marker genes described in previous studies (Bhaduri et al., 2020; Shi et al., 2021;
122 Uzquiano et al., 2022; Yu et al., 2021) (Fig 2A,B). Both genotypes contained radial glial
123 progenitors (RGP1 & 2), neuroectoderm progenitors (NEP), intermediate progenitors (IP),
124 immature neurons, projection neurons (PN), deep layer neurons (DLN), Cajal-Retzius cells (CR),
125 medial-like cells (MLC), inhibitory hindbrain neurons (IN hindbrain), cortical hem, and
126 mesenchyme. Additional cell types found only in *PAX6*$^{-/-}$ organoids include inhibitory neurons
127 (IN1 & 2), inhibitory neuron progenitors (IN progenitors), superficial layer neurons (SLN),
128 excitatory neurons (EN) which clustered separately from DLN or SLN and an additional cluster
129 of radial glial progenitors (RGP3) (Fig 2C,D).
130
131 Comparing the relative proportions of progenitor subtypes between *PAX6*$^{-/-}$ and control
132 organoids revealed a significant depletion of RGP1, RGP2 and IP in mutants (8-fold, almost 2-
133 fold and 8-fold decreases, respectively) and the presence of additional cell types RGP3 and IN
134 progenitors (Fig 2D). RGP1 and RGP2 expressed typical radial glial markers including *VIM*,
135 *FABP7* and *CLU*. RGP2 expressed active cell division markers including *TOP2A* and *MKI67*. RGP3,
136 in addition to *VIM*, *FABP7* and *CLU,* expressed genes not typically associated with RGPs
137 including *NPY* which is expressed by mature inhibitory neurons and *RORB* which is expressed
138 by layer 4 excitatory neurons, suggesting that this is an atypical RGP population caused by the
139 loss of PAX6 (Fig 2E).

140 There were also significant differences between the neuronal composition of *PAX6*$^{-/-}$ and
141 control organoids. Two clusters of inhibitory neuron types (IN1 and 2) were present in mutants,
142 but not controls (Fig 2C,D). These expressed genes associated with ventral telencephalic
143 identity, including *DLX2/5/6*, and *GAD1/2* and lacked expression of dorsal telencephalic
144 marker EMX1 (Fig 2B) (Supp table). Integration with published scRNAseq data from fetal
145 human ventral telencephalon (Yu et al., 2021) showed that IN1 and 2 cells are most similar to
146 interneuron precursors in the lateral and medial ganglionic eminences (LGE and MGE
147 respectively) (Supp Fig 2B,C).
148
149 *PAX6*$^{-/-}$ organoids also contained two excitatory neuron types (SLN and EN) not seen in controls
150 (Fig 2C,F) and contained fewer DLN and PN cells than controls (6:1 ratio compared to 3:1) (Fig
151 2F). This indicates PAX6 regulates DLN and PN production. SLN cells are relatively mature
152 neurons which express superficial layer markers including *SATB2* and *CUX2*, suggesting that
153 loss of PAX6 in human promotes accelerated differentiation of excitatory lineages, in contrast
154 to the delayed differentiation of cortical neurons seen in Pax6 mutant mice (Quintana-
155 Urzainqui et al., 2018). EN cells expressed genes associated with excitatory cortical neuronal
156 identity including *BCL11B* (*CTIP2*), *SCL17A6*, and *NEUROD6*. However, they also expressed
157 genes expressed medially such as CRABP1, and non-telencephalic genes including *PRDM13*
158 (spinal cord) (Supp table) – these cells are discussed further below.
159
160 ***Inhibitory cell types in PAX6*$^{-/-}$ *organoids arise through two distinct differentiation routes.***
161 To explore how the fate changes in *PAX6*$^{-/-}$ organoids arise, we used RNA Velocity analysis (La
162 Manno et al., 2018) to infer differentiation trajectories. This revealed that control organoids
163 generate excitatory neurons through two distinct routes, one from RGPs into IPs, then to
164 excitatory neurons and the other from NEPs directly into neurons (Fig. 2G), analogous to
165 known differentiation routes in both mouse (Götz and Huttner, 2005) and human (Eze et al.,
166 2021). RGP and NEP progenitors in *PAX6*$^{-/-}$ organoids both gave rise to excitatory and inhibitory
167 neurons. RGP3 proceed through IN progenitors ultimately giving rise to inhibitory neurons
168 while NEPs directly gave rise to inhibitory neurons (Fig 2H). Thus, in the absence of PAX6, both
169 NEP and RGP progenitors give rise to ectopic populations of inhibitory neurons.
170
171

172 ***Inhibitory and excitatory cell types in PAX6$^{-/-}$ organoids are physically segregated.***
173 Acute deletion of *Pax6* in mouse cortical progenitors causes a subset of these cells to adopt a
174 Gad1-positive inhibitory identity and segregate from excitatory-lineage cells in the cortical
175 plate, forming an ectopic mass (Manuel et al., 2022). To examine the distribution of ectopic
176 inhibitory cells in *PAX6$^{-/-}$* organoids, we immunostained cryosections of day 60 organoids for
177 TBR2 (EOMES) to label cortical IP cells ('dorsal' identity) and DLX2 to identify inhibitory cell
178 precursors ('ventral' identity) (Fig 3A). Sections throughout each individual organoid were
179 sampled and reconstructed to form 3D models (Fig 3A). Voxels in each reconstructed organoid
180 were assigned a value corresponding to their relative level of expression of TBR2 or DLX2,
181 giving a readout of dorsal versus ventral identity for cell clusters (Fig 3B, Supp. Fig 3). This
182 clearly identified distinct, separate dorsal (excitatory) and ventral (inhibitory) territories in
183 each *PAX6$^{-/-}$* organoid, analogous to those observed in mouse (Manuel et al., 2022).
184
185 ***Comparing transcriptomes of PAX6$^{-/-}$ organoid and Pax6$^{-/-}$cKO mice.***
186 To compare effects of PAX6 loss between human and mouse, we integrated the day 60 human
187 organoid scRNAseq dataset with our previous E14.5 cortex-specific *Pax6$^{-/-}$* mouse dataset
188 (Manuel et al., 2022) (Fig 3C,D). Co-clustering analysis showed that the ectopic cell types RGP3,
189 IN progenitors and IN1/2 found in *PAX6$^{-/-}$* organoids are transcriptionally similar to mouse
190 atypical progenitors (aP), ectopic GABAergic cell-progenitor (eGC-P) and ectopic GABAergic
191 cell-neuron (eGC-N) respectively (Fig. 3C black arrows, D). Thus, the extra inhibitory cell types
192 found in the organoid model resemble those described in the mouse model transcriptionally
193 as well as in their physical distribution.
194
195 EN cells, the additional group of excitatory cells found in human *PAX6$^{-/-}$* organoids, expressed
196 genes also found in DML-SLN cells in *Pax6$^{-/-}$* mice (Manuel et al., 2022) including *CRABP1*, *LHX9*
197 and *PRDM13* (Supp Table) suggesting that EN cells could be the human equivalent of mouse
198 DML-SLN cells. However, EN cells did not co-segregate with DML-SLN when integrated (Fig 3C
199 red arrows, D). To explore the basis of this divergence, we performed differential gene
200 expression (DGE) analysis between EN (organoid) and DML-SLN (mouse) cells, followed by GO
201 enrichment analysis. We found differences between EN and DML-SLN in GO terms pertaining
202 to intercellular signalling pathways, with protein kinases A & C, Notch and growth factor
203 signalling upregulated in EN cells compared to DML-SLN while Mapk and Wnt signalling were

204 upregulated in DML-SLN compared to EN cells (Fig 4A). Further, terms associated with
205 GABAergic neuron differentiation were also found, indicating that DML-SLN cells express more
206 ventral/GABAergic genes than EN do. Protein kinases A&C, Notch and growth factor signalling
207 pathways all influence cell growth and proliferation (Callender and Newton, 2017; Dagda and
208 Banerjee, 2015; Guo and Wang, 2009), while Wnt signalling is implicated in dorso-ventral
209 patterning of the forebrain in mice (Harrison-Uy and Pleasure, 2012). This could potentially
210 explain the higher expression of ventral telencephalic genes in DML-SLN compared to EN and
211 suggests that PAX6 may selectively influence distinct intercellular signalling pathways during
212 excitatory neuronal differentiation in mouse and human.
213
214 ***Multiple intercellular signalling pathways are dysregulated in PAX6$^{-/-}$ cerebral organoids.***
215 To investigate whether dysregulated intercellular signalling could underlie the diversification
216 from excitatory to inhibitory cell fate in *PAX6$^{-/-}$* organoids, we used the R package CellChat (Jin
217 et al., 2021) to quantitatively infer and analyse intercellular communication networks based
218 on the scRNAseq expression data. Significant interactions are identified based on expression
219 of ligands, receptors and cofactors using a permutation-based statistical test. The number of
220 predicted intercellular signalling interactions was considerably higher in *PAX6$^{-/-}$* organoids
221 than controls (Fig 4B), suggesting that, in the absence of PAX6, cells are more likely to engage
222 with signalling pathways that they do not normally interact with.
223
224 CellChat also calculates interaction strength (Fig 4C), a measure of the probability that
225 intercellular interactions are active, inferred using the law of mass action and integrating
226 scRNAseq data with CellChat's signalling molecule interaction database (Jin et al., 2021).
227 CellChat estimated a lower probability of communication between cells in mutant organoids
228 than controls (Fig 4C), suggesting that while *PAX6$^{-/-}$* cells are promiscuous in their ligand-
229 receptor interactions, these interactions may not necessarily result in functional output.
230 Nevertheless, our results align with our hypothesis that Pax6 acts to protect cells in developing
231 cortex against extraneous signalling, thereby maintaining the correct differentiation trajectory
232 (Manuel et al., 2022). CellChat analysis indicated that the Pleiotrophin (PTN) and Midkine (MK)
233 signalling pathways were dysregulated in *PAX6$^{-/-}$* organoids (Fig 4D). This is interesting as
234 neither of these pathways has previously been implicated in cortical development in mice.
235 Investigation of their roles could be a fruitful area for future research.

236

237 Analysis of DGE between control and *PAX6*$^{-/-}$ RGP1 and RGP2 cells revealed increased
238 expression of subpallial genes including *DLX1/2/5/6*, *GSX2*, *GAD1/2* indicating that RGP1 and
239 RGP2 in mutant organoids have mixed excitatory/inhibitory identity. Expression of *PTCH1* and
240 *JAG1*, components of the SHH and NOTCH signalling pathways respectively, were also
241 increased in *PAX6*$^{-/-}$ RGP1 (Fig 4E). Additionally, we found significant increase in the NOTCH
242 signalling ligands *DLL1* and *DLK1*, in *PAX6*$^{-/-}$ RGP2 (Fig 4F). SHH promotes ventral identity and
243 NOTCH signalling affects the balance between cell proliferation and differentiation (Nian and
244 Hou, 2022; Xu et al., 2010) while GSX2 and the DLXs encode transcription factors involved in
245 inhibitory cell fate acquisition (Kessaris et al., 2014). This indicates that changes in signalling
246 and transcription factor expression due to PAX6 loss in the progenitor populations may
247 together underlie the diversion of excitatory cell fate to an inhibitory one. Previously, we
248 found no evidence that the Shh or Notch pathways were disrupted in mouse *Pax6*$^{-/-}$ cortex
249 (Manuel et al., 2022), suggesting that loss of PAX6 may affect signalling pathways differently
250 in mouse and human cortical progenitors populations. However, it is possible that subtle
251 changes in expression of signalling pathway components in the *Pax6*$^{-/-}$ mouse cortex may have
252 fallen below the level of detection, due to a lower sequencing depth compared to the current
253 study (Manuel et al., 2022).

254

255 Overall, we have shown that PAX6 loss leads to a subset of developing human cortical
256 progenitors deviating from excitatory to inhibitory fate. These ectopic cells in *PAX6*$^{-/-}$ organoids
257 strongly resembled equivalent cells described in *Pax6* mutant mice both transcriptomically
258 and in their distribution (Manuel et al., 2022). We found evidence of dysregulated signalling
259 pathways in progenitors that could underlie the observed fate change which were not
260 previously reported in mice. Thus, while the major role of PAX6 in preserving cortical
261 progenitors on the excitatory differentiation path remains conserved, our study suggests the
262 presence of mechanistic species-specific differences that warrant further exploration.

263 **Figure legends**

264

265 **Fig 1** (A) Diagram showing part of the human *PAX6* locus indicating the location and nature of
266 the mutation introduced to the *PAX6*$^{-/-}$ iPSC lines. Homozygous insertion of a single T residue
267 in exon 4 caused a frameshift mutation leading to a premature stop codon within exon 4.
268 Exons 1-3 are non-coding. PD – paired domain; LNK – linker; HD – homeodomain; TAD –
269 transactivation domain. (B) Sanger sequencing of *PAX6*$^{-/-}$ iPSC genomic DNA showing the T
270 insertion mutation. (C) PAX6 PD immunostaining of day 60 control and *PAX6*$^{-/-}$ organoids,
271 confirming PAX6 protein absence in mutants. (D,E) SOX2 and N-CAD Immunostaining of
272 representative sections of individual day 60 control and *PAX6*$^{-/}$organoids. Scale bar = 1mm. (F)
273 Quantification of cross-sectional area of day 60 control and *PAX6*$^{-/-}$ organoids. (G–J)
274 Quantification of organoid size and rosette characteristics. Each symbol represents an
275 individual organoid while triangles, dots and square symbols indicate separate organoid
276 batches.

277

278 **Fig 2** (A) UMAP plot showing combined scRNAseq data from day 60 *PAX6*$^{-/-}$ and control
279 organoids. RGP – Radial glia progenitor; IP – Intermediate progenitor; IN Progenitor –
280 Inhibitory progenitor; IN – Inhibitory neuron; CR – Cajal-Retzius cells; IN Hindbrain – Inhibitory
281 hindbrain; MLC – Medial-like cells; PN – Projection neurons; NEP – Neuroectodermal
282 progenitors; EN – excitatory neuron; DLN – Deep layer neuron; SLN – Superficial layer neuron
283 (B) Violin plots showing selected marker gene expression in specific cell types in day 60
284 organoids. (C) Separate UMAP plots of scRNAseq data from control (left) and *PAX6*$^{-/-}$ (right)
285 organoids. (D-F) Comparison of cell type composition between control and *PAX6*$^{-/-}$ day 60
286 organoids showing all cell types (D), progenitors only (E) and neuronal cell types only (F). (G,H)
287 RNA Velocity analysis of day 60 *PAX6*$^{-/-}$ and control organoids, abbreviations as in (A).

288

289 **Fig 3** (A) Schema outlining method for production and quantitation of 3D models of organoids.
290 Sections were immunostained for TBR2 and DLX2 and processed as shown. (B) Equation by
291 which dorsal/ventral identities were conferred upon specific territories in organoids and graph
292 summarising the segregation of these territories in individual organoids. (C,D) Integration of
293 current day 60 human organoid scRNAseq data with E14.5 mouse scRNAseq data from Manuel
294 *et al*., 2022. Cell clusters identified in mice are labelled in red and human clusters in black.

295 Black arrows indicate cell types that are similar between human and mouse while red arrows
296 show cell types that are transcriptomically distant. (D) Cells from human organoids are shown
297 in red and mouse cells in blue.
298
299 **Fig 4** (A) GO enrichment analysis of genes differentially expressed between the extra
300 excitatory cell types found in human *PAX6*$^{-/-}$ organoids (EN) and E14.5 mouse (DML-SLN)
301 samples. (B,C) CellChat analysis comparing number and strength of inferred intercellular
302 signalling interactions in day 60 *PAX6*$^{-/-}$ and control organoids. (D) Graph depicting the relative
303 interaction strength of specific signalling pathways between control and *PAX6*$^{-/}$ organoids. (E,F)
304 Volcano plots showing genes differentially expressed in RGP1 and RGP2 populations.
305
306 **Supp Fig 1.** (A) Immunostaining of Crispr edited iPSC cell lines used in this study showing
307 expression of pluripotency markers NANOG, OCT3/4 and TRA-1-60. HeLa cells were used as a
308 negative control. (B) Timeline illustrating organoid differentiation protocol.
309
310 **Supp Fig 2.** (A) UMAP plots for each organoid sample submitted for scRNAseq. In this initial
311 analysis, distinct clusters are colour-coded but specific cell type identities were not assigned.
312 Asterisks indicate outlier samples which were removed prior to downstream analysis. (B)
313 Integration of day 60 human *PAX6*$^{-/-}$ and control organoid scRNAseq dataset with published
314 fetal human ventral telencephalon scRNAseq data (Yu et al., 2021) to assign identities to
315 specific clusters (C) Human organoid clusters labelled in black text and human fetal clusters in
316 red.
317
318 **Supp Fig 3.** 3D models of all individual organoids of both *PAX6*$^{-/-}$ clones (A10 and B2) that were
319 quantified.
320
321 **Supp Table**. Marker genes of each cluster listed in individual cluster tabs. DGE and GO
322 enrichment analysis results are available as individual tabs.

323 **Material & Methods**

324

325 *Cell culture and organoid generation*

326 iPSCs were maintained at 37°C with 5% CO_2 in StemMACS iPS-Brew XF (Miltenyi) on Laminin
327 521 (Biolamina) coated plates and passaged with 0.5 mM EDTA (Life Technologies). Organoids
328 were differentiated using a modified Lancaster protocol (Lancaster et al., 2013) which included
329 addition of 10µM SB431542 (Tocris) and 100nM LDN-193189 (APExBIO) for neural induction
330 and addition of 20ng/ml BDNF and NT3 (Peprotech) to the medium at D30 for two weeks to
331 aid neuronal maturation. Organoids were maintained in 37°C with 5% CO_2 incubators on
332 shakers for 60 days and all media change were done every other day.

333

334 *CRISPR/Cas9 mutagenesis*

335 iPSCs were transfected with sgRNA 3' UCCCUUUCCUCAGGUCACAG 5' (Synthego) via
336 nucleofection using program CA137 on a 4D Nucleofactor X (Lonza) as per manufacturer's
337 instructions. Clones were obtained by single cell dissociation of the transfected pool followed
338 by screening for PAX6 mutation by Sanger sequencing of the *PAX6* locus. Successfully edited
339 clones were re-sequenced and pluripotency test were performed using STEMlight
340 Pluripotency kit (Invitrogen) (Supp Fig 1). Likely sites for off-target effects were identified using
341 Cas-OFFinder (http://www.rgenome.net/cas-offinder/) and annotated in whole genome
342 sequencing (WGS) data of all the iPSC lines. WGS data of all cell lines are deposited in ENA
343 (accession: PRJEB63603).

344

345 *Immunohistochemistry*

346 12µm thick cryosections of organoids were permeabilized in 0.1% Triton/PBS before
347 incubation with primary antibodies at 1/200 dilution using appropriate serum as blocking
348 buffer without antigen retrieval step: SOX2 (rabbit, ab92494 Abcam), TBR2 (sheep, AF6166
349 Bio-Techne), DLX2 (mouse, sc-393879 Santa Cruz); with antigen retrieval step: PAX6 (mouse,
350 AD2.38, described in Engelkamp et al., (1999)), NCAD (mouse, 610920 BD Biosciences). All
351 primary antibodies (except PAX6) were detected using AlexaFluor secondary antibodies
352 (Invitrogen) at 1/200 dilution. PAX6 was detected using Vectastain ABC kit (Vector Labs).
353 StemLight Pluripotency Antibody Kit (Stem Cell Technologies) was used for pluripotency

354 testing. All immunohistochemistry was performed on ≥ 3 sections of individual control and
355 *PAX6*$^{-/-}$ organoids.
356
357 *3D modelling*
358 Every 16th section of individual organoids labelled with TBR2 and DLX2 was sampled using
359 Zeiss Axio Scan Z1 slide scanner. A 200 x 200 µm grid was superimposed on each section and
360 fluorescent intensities corresponding to both DLX2 and TBR2 expression were measured for
361 each square. Expression data was then voxelised by assigning three-dimensional coordinates
362 to each grid square. Voxels were processed using the 3D modelling package Plotly (Sievert,
363 2020) to produce 3D heatmaps of TBR2 and DLX2 expression in each organoid. To determine
364 whether excitatory and inhibitory cells were mixed or segregated, voxels of TBR2 and DLX2
365 expression were used to calculate a DV value, given by the formula: log TBR2/DLX2 intensities
366 (Fig. 3B). This gave a value range to allow plotting 'dorsal' areas, which contain excitatory
367 neurons and 'ventral' areas where inhibitory neurons are enriched.
368
369 *Organoid dissociation and single cell RNA sequencing*
370 Four organoids of each genotype from four separate differentiation batches were submitted
371 for scRNAseq. Briefly, organoids were cut into smaller pieces with a scalpel and incubated at
372 37°C in papain solution (Worthington) for 30 minutes (Velasco et al., 2019) before single cell
373 resuspension for downstream processing using 10X Genomics Chromium Next GEM Single Cell
374 3' Reagent Kits v3.1 as per manufacturer's instruction. Sequencing was performed using
375 Ilumina NovaSeq.
376
377 Raw sequences were processed using the CellRanger pipeline 6.1.1 and ambient RNA reads
378 were removed using SoupX (Young and Behjati, 2020). Cells expressing <500 or >8000 genes
379 and/or 25% mitochondrial genes were excluded. Standard downstream processing of
380 scRNAseq datasets was performed using Seurat v.4.0 (Hao et al., 2021). Integration of datasets
381 with publicly available dataset was achieved using FindIntegrationAnchors() and
382 IntegrateData() commands from Seurat. Mouse gene names were converted to human
383 equivalents using orthogene (Schilder, 2023) before integration. Pseudobulking for DESeq2
384 (Love et al., 2014) differential gene analysis was achieved using the AggregateBioVar package
385 (Thurman et al., 2021). RNA velocity was estimated using scVelo (Bergen et al., 2020; La

386 Manno et al., 2018) and cell-cell signalling interaction inferencing was performed using
387 CellChat (Jin et al., 2021). Raw sequences deposited in ENA (PRJEB63603).
388
389 *Statistical analysis*
390 For each between-organoid comparison (Control vs *PAX6*$^{-/-}$), an ANOVA with nested mixed
391 effects was performed, accounting for the random effect of batches and clones on variance in
392 a hierarchical manner. Specifically, p-values and confidence intervals were calculated using a
393 Type III Analysis of Variance with Satterthwaite's method.
394
395 **Acknowledgements**
396 We thank Tilo Kunath for sharing the NAS2 hIPSC line. We are grateful to Michela Barbato for
397 skilled assistance in cell culture, Thomas Theil, and Thomas Pratt for helpful comments on the
398 manuscript. This work was supported by Simons Initiative for the Developing Brain (grant
399 number 529085).
400
401 **References**
402
403 Bamiou, D.-E., Free, S. L., Sisodiya, S. M., Chong, W. K., Musiek, F., Williamson, K. A., van
404 Heyningen, V., Moore, A. T., Gadian, D. and Luxon, L. M. (2007). Auditory interhemispheric
405 transfer deficits, hearing difficulties, and brain magnetic resonance imaging abnormalities in
406 children with congenital aniridia due to PAX6 mutations. *Archives of pediatrics & adolescent*
407 *medicine* 161, 463–9.
408 Bergen, V., Lange, M., Peidli, S., Wolf, F. A. and Theis, F. J. (2020). Generalizing RNA velocity
409 to transient cell states through dynamical modeling. *Nat Biotechnol* 38, 1408–1414.
410 Bhaduri, A., Andrews, M. G., Leon, W. M., Jung, D., Shin, D., Allen, D., Jung, D., Schmunk, G.,
411 Haeussler, M., Salma, J., et al. (2020). Cell stress in cortical organoids impairs molecular
412 subtype specification. *Nature* 578, 142–148.
413 Birey, F., Andersen, J., Makinson, C. D., Islam, S., Wei, W., Huber, N., Fan, H. C., Metzler, K. R.
414 C., Panagiotakos, G., Thom, N., et al. (2017). Assembly of functionally integrated human
415 forebrain spheroids. *Nature* 545, 54–59.
416 Bruining, H., Hardstone, R., Juarez-Martinez, E. L., Sprengers, J., Avramiea, A.-E., Simpraga,
417 S., Houtman, S. J., Poil, S.-S., Dallares, E., Palva, S., et al. (2020). Measurement of excitation-
418 inhibition ratio in autism spectrum disorder using critical brain dynamics. *Sci Rep* 10, 9195.
419 Cadwell, C. R., Bhaduri, A., Mostajo-Radji, M. A., Keefe, M. G. and Nowakowski, T. J. (2019).
420 Development and Arealization of the Cerebral Cortex. *Neuron* 103, 980–1004.
421 Callender, J. A. and Newton, A. C. (2017). Conventional protein kinase C in the brain: 40
422 years later. *Neuronal Signal* 1, NS20160005.

Chambers, S. M., Fasano, C. A., Papapetrou, E. P., Tomishima, M., Sadelain, M. and Studer, L. (2009). Highly efficient neural conversion of human ES and iPS cells by dual inhibition of SMAD signaling. *Nature biotechnology* 27, 275–280.

Dagda, R. K. and Banerjee, T. D. (2015). Role of PKA in regulating mitochondrial function and neuronal development: implications to neurodegenerative diseases. *Rev Neurosci* 26, 359–370.

Devine, M. J., Ryten, M., Vodicka, P., Thomson, A. J., Burdon, T., Houlden, H., Cavaleri, F., Nagano, M., Drummond, N. J., Taanman, J.-W. W., et al. (2011). Parkinson's disease induced pluripotent stem cells with triplication of the α-synuclein locus. *Nature Communications* 2, 440.

Engelkamp, D., Rashbass, P., Seawright, A. and Heyningen, V. van (1999). Role of Pax6 in development of the cerebellar system. *Development* 126, 3585–3596.

Eze, U. C., Bhaduri, A., Haeussler, M., Nowakowski, T. J. and Kriegstein, A. R. (2021). Single-cell atlas of early human brain development highlights heterogeneity of human neuroepithelial cells and early radial glia. *Nat Neurosci* 24, 584–594.

Glaser, T., Jepeal, L., Edwards, J. G., Young, S. R., Favor, J. and Maas, R. L. (1994). PAX6 gene dosage effect in a family with congenital cataracts, aniridia, anophthalmia and central nervous system defects. *Nat Genet* 7, 463–471.

Gomes, A. R., Fernandes, T. G., Vaz, S. H., Silva, T. P., Bekman, E. P., Xapelli, S., Duarte, S., Ghazvini, M., Gribnau, J., Muotri, A. R., et al. (2020). Modeling Rett Syndrome With Human Patient-Specific Forebrain Organoids. *Frontiers in Cell and Developmental Biology* 8,.

Götz, M. and Huttner, W. B. (2005). The cell biology of neurogenesis. *Nature reviews. Molecular cell biology* 6, 777–788.

Guo, X. and Wang, X.-F. (2009). Signaling cross-talk between TGF-β/BMP and other pathways. *Cell Res* 19, 71–88.

Hao, Y., Hao, S., Andersen-Nissen, E., Mauck, W. M., Zheng, S., Butler, A., Lee, M. J., Wilk, A. J., Darby, C., Zager, M., et al. (2021). Integrated analysis of multimodal single-cell data. *Cell* 184, 3573-3587.e29.

Harrison-Uy, S. J. and Pleasure, S. J. (2012). Wnt Signaling and Forebrain Development. *Cold Spring Harb Perspect Biol* 4, a008094.

Haubst, N., Berger, J., Radjendirane, V., Graw, J., Favor, J., Saunders, G. F., Stoykova, A. and Götz, M. (2004). Molecular dissection of Pax6 function: The specific roles of the paired domain and homeodomain in brain development. *Development* 131, 6131–6140.

Holm, P. C., Mader, M. T., Haubst, N., Wizenmann, A., Sigvardsson, M. and Götz, M. (2007). Loss- and gain-of-function analyses reveal targets of Pax6 in the developing mouse telencephalon. *Molecular and cellular neurosciences* 34, 99–119.

Jin, S., Guerrero-Juarez, C. F., Zhang, L., Chang, I., Ramos, R., Kuan, C.-H., Myung, P., Plikus, M. V. and Nie, Q. (2021). Inference and analysis of cell-cell communication using CellChat. *Nat Commun* 12, 1088.

Kessaris, N., Magno, L., Rubin, A. N. and Oliveira, M. G. (2014). Genetic programs controlling cortical interneuron fate. *Current Opinion in Neurobiology* 26, 79–87.

Kroll, T. T. and O'Leary, D. D. M. (2005). Ventralized dorsal telencephalic progenitors in Pax6 mutant mice generate GABA interneurons of a lateral ganglionic eminence fate. *Proceedings of the National Academy of Sciences of the United States of America* 102, 7374–7379.

La Manno, G., Soldatov, R., Zeisel, A., Braun, E., Hochgerner, H., Petukhov, V., Lidschreiber, K., Kastriti, M. E., Lönnerberg, P., Furlan, A., et al. (2018). RNA velocity of single cells. *Nature* 560, 494–498.

Lancaster, M. A., Renner, M., Martin, C.-A. A., Wenzel, D., Bicknell, L. S., Hurles, M. E., Homfray, T., Penninger, J. M., Jackson, A. P. and Knoblich, J. A. (2013). Cerebral organoids model human brain development and microcephaly. *Nature* 501, 373-+.

Love, M. I., Huber, W. and Anders, S. (2014). Moderated estimation of fold change and dispersion for RNA-seq data with DESeq2. *Genome Biology* 15, 550.

Manuel, M. N., Mi, D., Masonand, J. O. and Price, D. J. (2015). Regulation of cerebral cortical neurogenesis by the Pax6 transcription factor. *Frontiers in Cellular Neuroscience* 9,.

Manuel, M., Tan, K. B., Kozic, Z., Molinek, M., Marcos, T. S., Razak, M. F. A., Dobolyi, D., Dobie, R., Henderson, B. E. P., Henderson, N. C., et al. (2022). Pax6 limits the competence of developing cerebral cortical cells to respond to inductive intercellular signals. *PLOS Biology* 20, e3001563.

Nian, F.-S. and Hou, P.-S. (2022). Evolving Roles of Notch Signaling in Cortical Development. *Frontiers in Neuroscience* 16,.

Ochi, S., Manabe, S., Kikkawa, T. and Osumi, N. (2022). Thirty Years' History since the Discovery of Pax6: From Central Nervous System Development to Neurodevelopmental Disorders. *Int J Mol Sci* 23, 6115.

Quintana-Urzainqui, I., Kozić, Z., Mitra, S., Tian, T., Manuel, M., Mason, J. O. and Price, D. J. (2018). Tissue-Specific Actions of Pax6 on Proliferation and Differentiation Balance in Developing Forebrain Are Foxg1 Dependent. *iScience* 10, 171–191.

Scardigli, R., Bäumer, N., Gruss, P., Guillemot, F. and Le Roux, I. (2003). Direct and concentration-dependent regulation of the proneural gene Neurogenin2 by Pax6. *Development* 130, 3269–3281.

Schilder, B. (2023). orthogene: Interspecies gene mapping.

Schmidt-Sidor, B., Szymańska, K., Williamson, K., van Heyningen, V., Roszkowski, T., Wierzba-Bobrowicz, T. and Zaremba, J. (2009). Malformations of the brain in two fetuses with a compound heterozygosity for two PAX6 mutations. *Folia Neuropathol* 47, 372–382.

Shi, Y., Wang, M., Mi, D., Lu, T., Wang, B., Dong, H., Zhong, S., Chen, Y., Sun, L., Zhou, X., et al. (2021). Mouse and human share conserved transcriptional programs for interneuron development. *Science (New York, N.Y.)* 374, eabj6641.

Sievert, C. (2020). *Interactive Web-Based Data Visualization with R, plotly, and shiny*. Boca Raton: Chapman and Hall/CRC.

Sisodiya, S. M., Free, S. L., Williamson, K. A., Mitchell, T. N., Willis, C., Stevens, J. M., Kendall, B. E., Shorvon, S. D., Hanson, I. M., Moore, A. T., et al. (2001). PAX6 haploinsufficiency causes cerebral malformation and olfactory dysfunction in humans. *Nat Genet* 28, 214–216.

Solomon, B. D., Pineda-Alvarez, D. E., Balog, J. Z., Hadley, D., Gropman, A. L., Nandagopal, R., Han, J. C., Hahn, J. S., Blain, D., Brooks, B., et al. (2009). Compound heterozygosity for mutations in PAX6 in a patient with complex brain anomaly, neonatal diabetes mellitus, and microophthalmia. *American Journal of Medical Genetics, Part A* 149, 2543–2546.

Terzić, J. and Saraga-Babić, M. (1999). Expression pattern of PAX3 and PAX6 genes during human embryogenesis. *Int J Dev Biol* 43, 501–508.

Thompson, P. J., Mitchell, T. N., Free, S. L., Williamson, K. A., Hanson, I. M., van Heyningen, V., Moore, A. T. and Sisodiya, S. M. (2004). Cognitive functioning in humans with mutations of the PAX6 gene. *Neurology* 62, 1216–1218.

Thurman, A. L., Ratcliff, J. A., Chimenti, M. S. and Pezzulo, A. A. (2021). Differential gene expression analysis for multi-subject single-cell RNA-sequencing studies with aggregateBioVar. *Bioinformatics* 37, 3243–3251.

Toresson, H., Parmar, M. and Campbell, K. (2000). Expression of Meis and Pbx genes and their protein products in the developing telencephalon: Implications for regional differentiation. *Mechanisms of Development* 94, 183–187.

Traag, V. A., Waltman, L. and van Eck, N. J. (2019). From Louvain to Leiden: guaranteeing well-connected communities. *Scientific Reports* 9,.

Tzoulaki, I., White, I. M. and Hanson, I. M. (2005). PAX6 mutations: genotype-phenotype correlations. *BMC Genet* 6, 27.

Uzquiano, A., Kedaigle, A. J., Pigoni, M., Paulsen, B., Adiconis, X., Kim, K., Faits, T., Nagaraja, S., Antón-Bolaños, N., Gerhardinger, C., et al. (2022). Proper acquisition of cell class identity in organoids allows definition of fate specification programs of the human cerebral cortex. *Cell* 185, 3770-3788.e27.

Velasco, S., Kedaigle, A. J., Simmons, S. K., Nash, A., Rocha, M., Quadrato, G., Paulsen, B., Nguyen, L., Adiconis, X., Regev, A., et al. (2019). Individual brain organoids reproducibly form cell diversity of the human cerebral cortex. *Nature* 570, 523–527.

Walcher, T., Xie, Q., Sun, J., Irmler, M., Beckers, J., Öztürk, T., Niessing, D., Stoykova, A., Cvekl, A., Ninkovic, J., et al. (2013). Functional dissection of the paired domain of Pax6 reveals molecular mechanisms of coordinating neurogenesis and proliferation. *Development (Cambridge)* 140, 1123–1136.

Walther, C. and Gruss, P. (1991). Pax-6, a murine paired box gene, is expressed in the developing CNS. *Development* 113, 1435–1450.

Xu, Q., Guo, L., Moore, H., Waclaw, R. R., Campbell, K. and Anderson, S. A. (2010). Sonic hedgehog signaling confers ventral telencephalic progenitors with distinct cortical interneuron fates. *Neuron* 65, 328–340.

Yogarajah, M., Matarin, M., Vollmar, C., Thompson, P. J., Duncan, J. S., Symms, M., Moore, A. T., Liu, J., Thom, M., van Heyningen, V., et al. (2016). PAX6, brain structure and function in human adults: Advanced MRI in aniridia. *Annals of Clinical and Translational Neurology* 3, 314–330.

Young, M. D. and Behjati, S. (2020). SoupX removes ambient RNA contamination from droplet-based single-cell RNA sequencing data. *GigaScience* 9, giaa151.

Yu, Y., Zeng, Z., Xie, D., Chen, R., Sha, Y., Huang, S., Cai, W., Chen, W., Li, W., Ke, R., et al. (2021). Interneuron origin and molecular diversity in the human fetal brain. *Nature Neuroscience* 24, 1745–1756.

Zhang, X., Huang, C. T., Chen, J., Pankratz, M. T., Xi, J., Li, J., Yang, Y., LaVaute, T. M., Li, X. J., Ayala, M., et al. (2010). Pax6 is a human neuroectoderm cell fate determinant. *Cell Stem Cell* 7, 90–100.

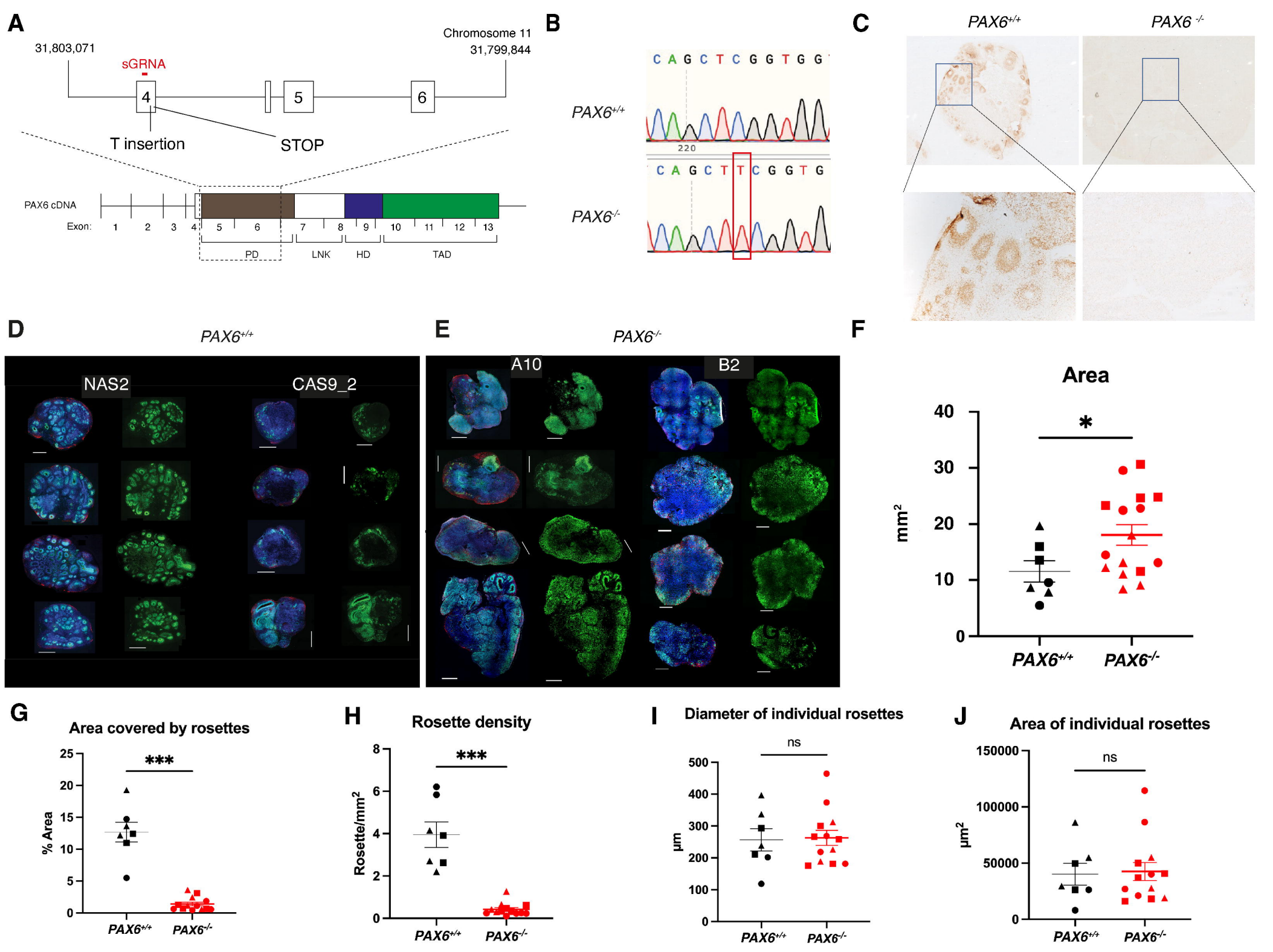
A
31,803,071
Chromosome 11
31,799,844
sGRNA
4
5
6
T insertion
STOP
PAX6 cDNA
Exon: 1 2 3 4 5 6 7 8 9 10 11 12 13
PD
LNK
HD
TAD
B
PAX6+/+
PAX6-/-
C A G C T C G G T G G
220
C A G C T T C G G T G
C
PAX6+/+
PAX6 -/-
D
PAX6+/+
NAS2
CAS9_2
E
PAX6-/-
A10
B2
F
Area
mm2
40
30
20
10
0
*
PAX6+/+
PAX6-/-
G
Area covered by rosettes
% Area
25
20
15
10
5
0
***
PAX6+/+
PAX6-/-
H
Rosette density
Rosette/mm2
8
6
4
2
0
***
PAX6+/+
PAX6-/-
I
Diameter of individual rosettes
µm
500
400
300
200
100
0
ns
PAX6+/+
PAX6-/-
J
Area of individual rosettes
µm2
150000
100000
50000
0
ns
PAX6+/+
PAX6-/-

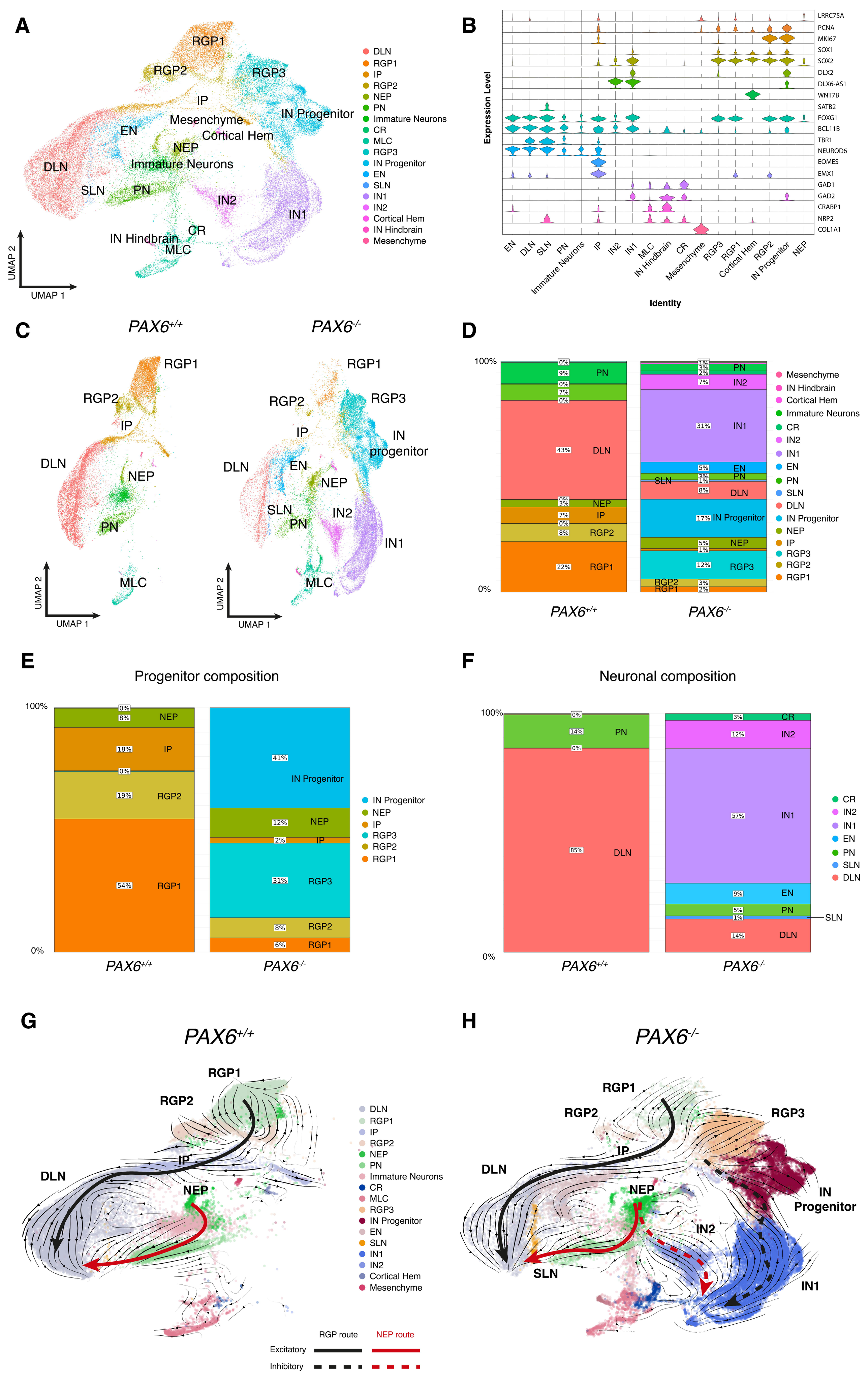
A
RGP1
RGP2
RGP3
IP
Mesenchyme
IN Progenitor
EN
Cortical Hem
NEP
DLN
Immature Neurons
SLN
PN
IN2
IN1
CR
IN Hindbrain
MLC
UMAP 2
UMAP 1
DLN
RGP1
IP
RGP2
NEP
PN
Immature Neurons
CR
MLC
RGP3
IN Progenitor
EN
SLN
IN1
IN2
Cortical Hem
IN Hindbrain
Mesenchyme
B
Expression Level
LRRC75A
PCNA
MKI67
SOX1
SOX2
DLX2
DLX6-AS1
WNT7B
SATB2
FOXG1
BCL11B
TBR1
NEUROD6
EOMES
EMX1
GAD1
GAD2
CRABP1
NRP2
COL1A1
EN
DLN
SLN
PN
Immature Neurons
IP
IN2
IN1
MLC
IN Hindbrain
CR
Mesenchyme
RGP3
RGP1
Cortical Hem
RGP2
IN Progenitor
NEP
Identity
C
PAX6+/+
PAX6-/-
RGP1
RGP2
IP
DLN
NEP
PN
MLC
UMAP 2
UMAP 1
RGP1
RGP2
RGP3
IP
IN progenitor
DLN
EN
NEP
SLN
IN2
PN
IN1
MLC
UMAP 2
UMAP 1
D
100%
0%
0%
9%
0%
7%
0%
43%
0%
3%
7%
0%
8%
22%
PN
DLN
NEP
IP
RGP2
RGP1
1%
3%
2%
7%
31%
5%
3%
1%
8%
17%
5%
1%
12%
3%
2%
PN
IN2
IN1
EN
PN
SLN
DLN
IN Progenitor
NEP
RGP3
RGP2
RGP1
PAX6+/+
PAX6-/-
Mesenchyme
IN Hindbrain
Cortical Hem
Immature Neurons
CR
IN2
IN1
EN
PN
SLN
DLN
IN Progenitor
NEP
IP
RGP3
RGP2
RGP1
E
Progenitor composition
100%
0%
0%
8%
18%
0%
19%
54%
NEP
IP
RGP2
RGP1
41%
12%
2%
31%
8%
6%
IN Progenitor
NEP
IP
RGP3
RGP2
RGP1
IN Progenitor
NEP
IP
RGP3
RGP2
RGP1
PAX6+/+
PAX6-/-
F
Neuronal composition
100%
0%
0%
14%
0%
85%
PN
DLN
3%
12%
57%
9%
5%
1%
14%
CR
IN2
IN1
EN
PN
SLN
DLN
CR
IN2
IN1
EN
PN
SLN
DLN
PAX6+/+
PAX6-/-
G
PAX6+/+
RGP1
RGP2
IP
DLN
NEP
DLN
RGP1
IP
RGP2
NEP
PN
Immature Neurons
CR
MLC
RGP3
IN Progenitor
EN
SLN
IN1
IN2
Cortical Hem
Mesenchyme
RGP route
NEP route
Excitatory
Inhibitory
H
PAX6-/-
RGP1
RGP2
RGP3
IP
DLN
NEP
IN Progenitor
IN2
SLN
IN1

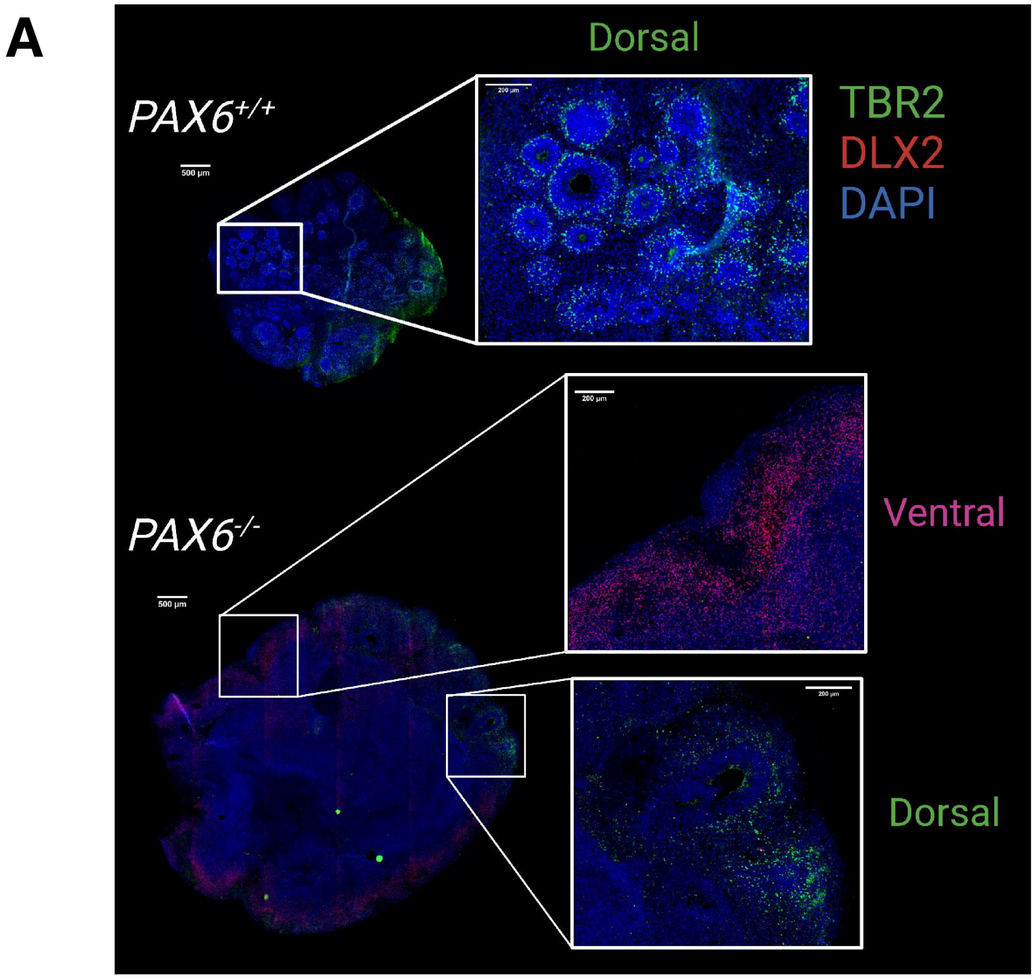

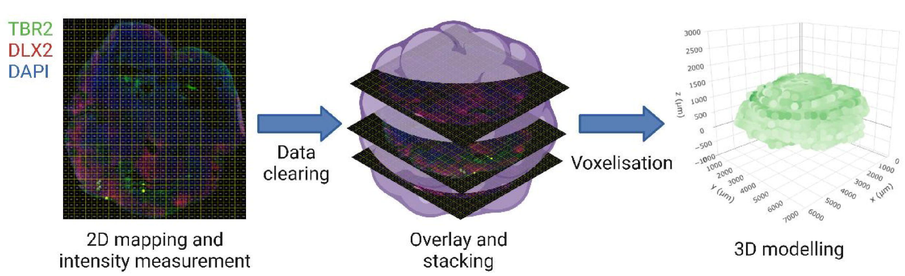

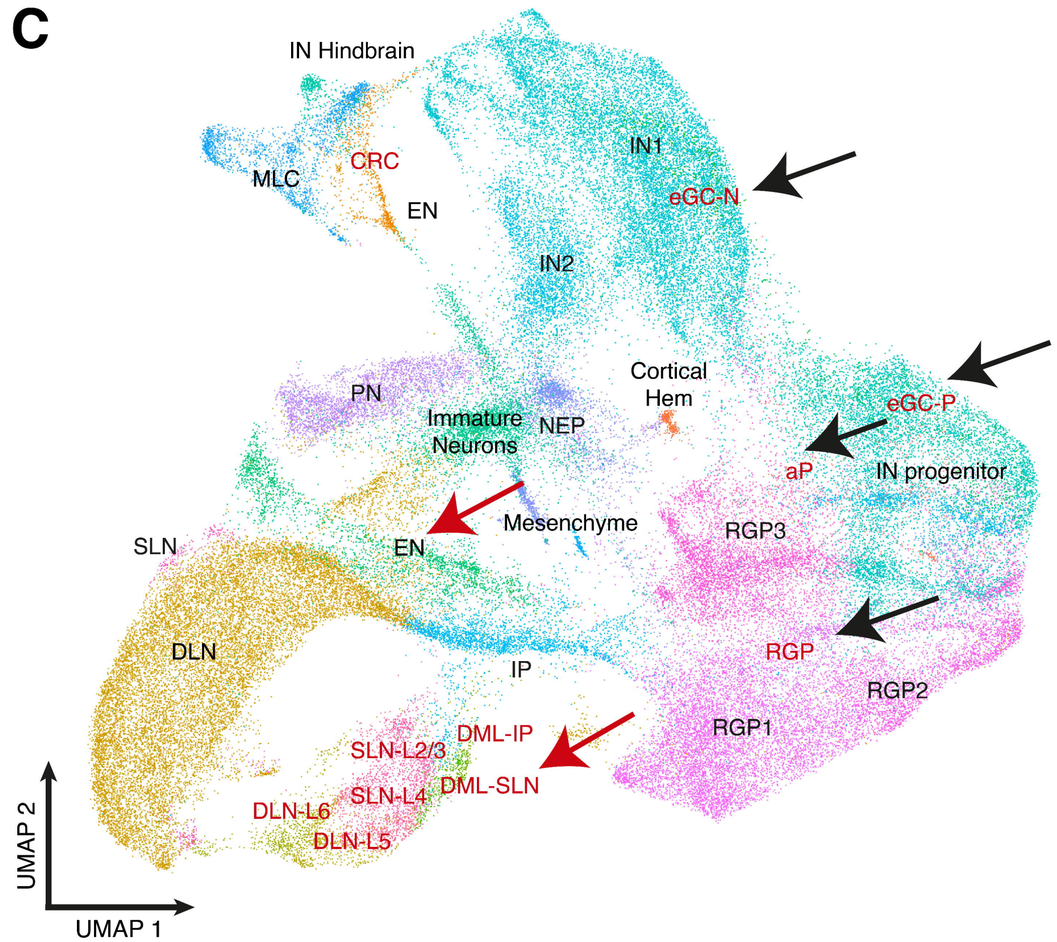

Human	Mouse
IN1	aP
IN2	RGP
IP	CRC
Mesenchyme	SLN-L2/3
MLC	SLN-L4
NEP	DLN-L5
PN	DLN-L6
RGP1	DML-IP
RGP2	DML-SLN
RGP3	eGC-N
SLN	eGC-P
DLN	
EN	
Immature Neurons	
IN Hindbrain	
IN progenitor	
Cortical Hem	
CR	

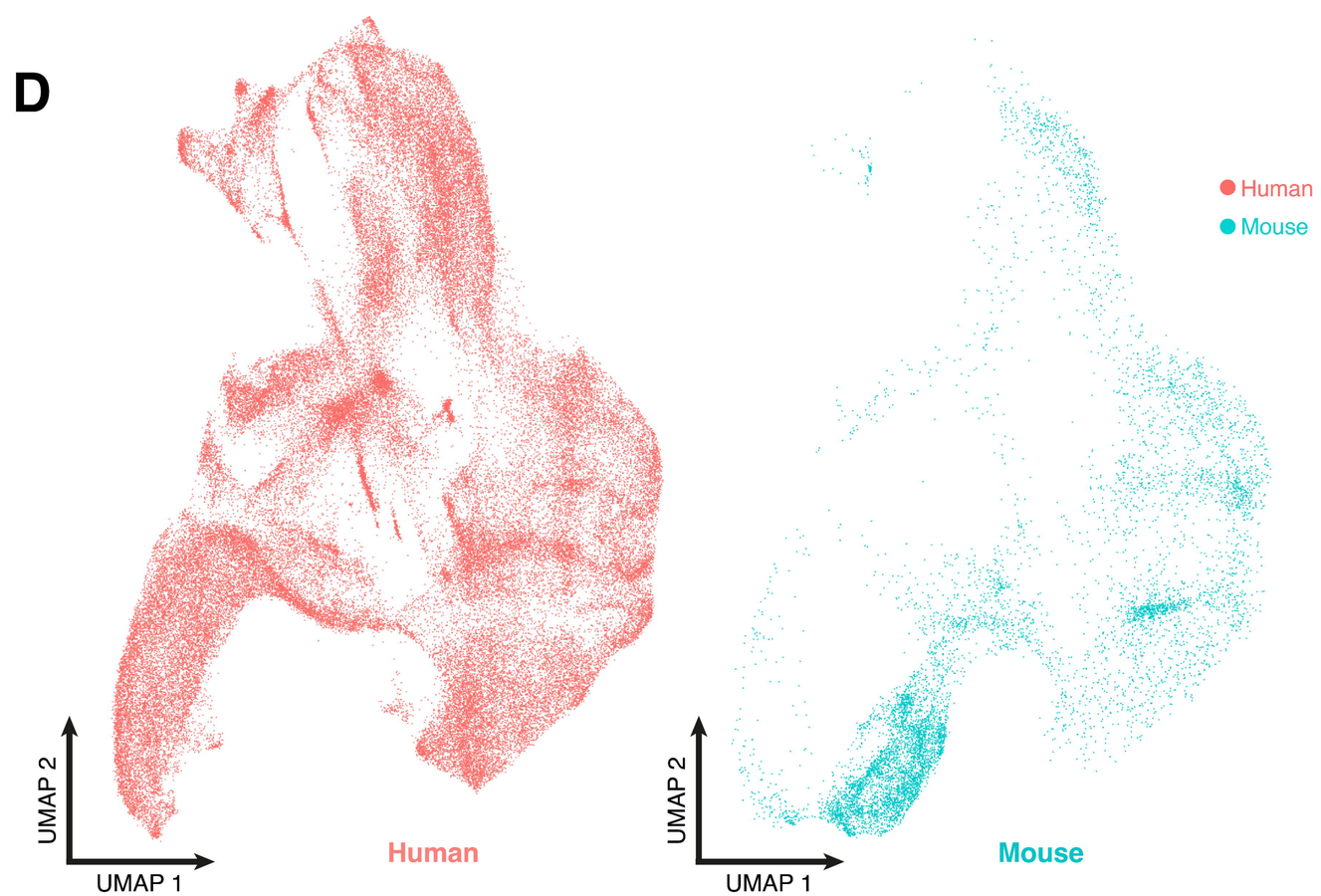

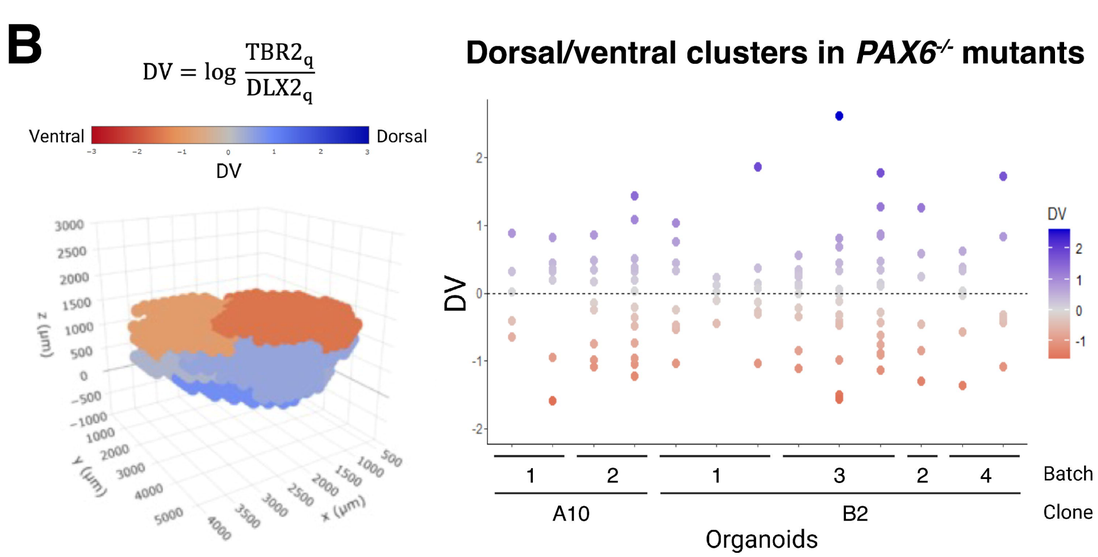

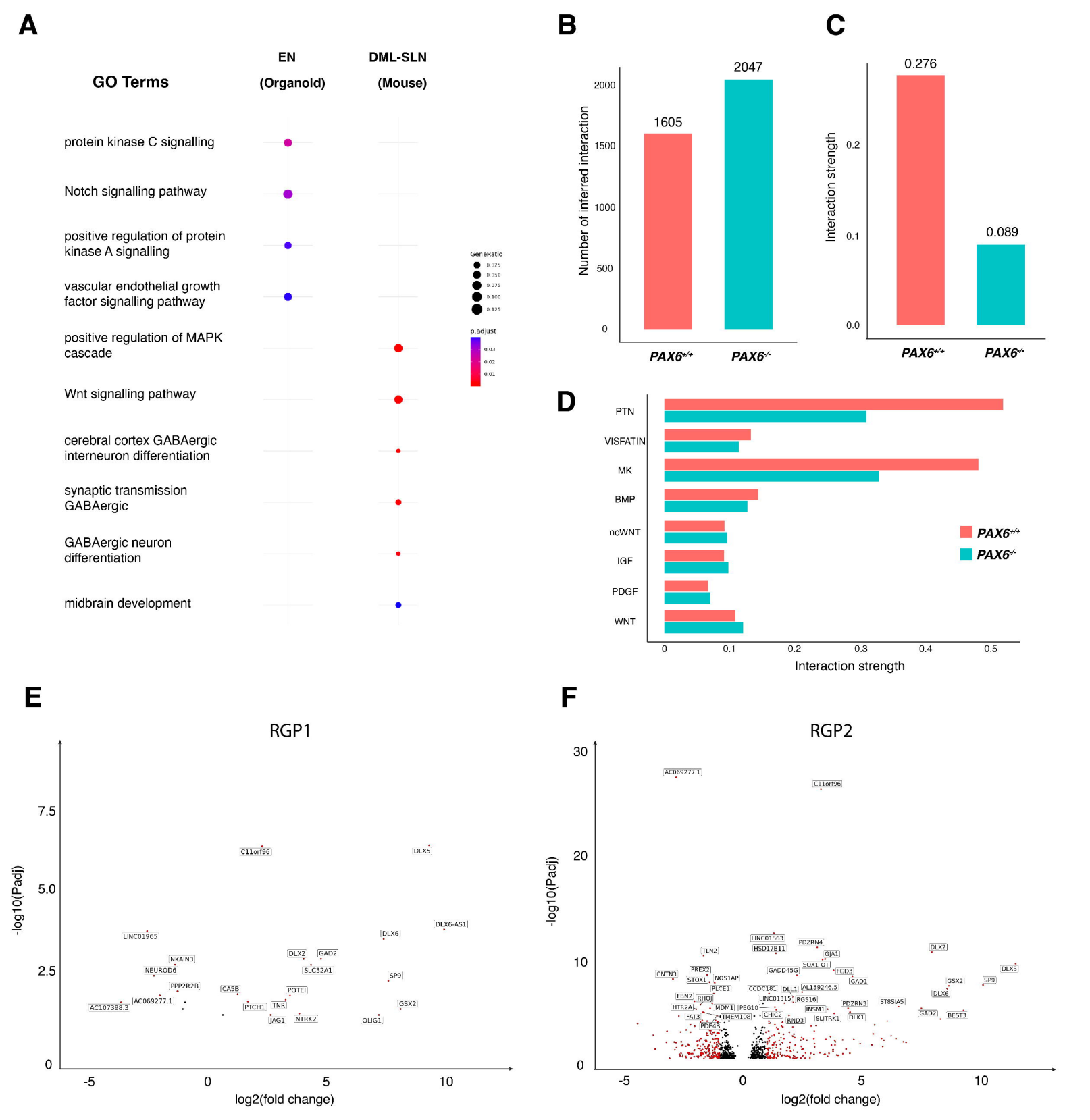
A
GO Terms
EN
(Organoid)
DML-SLN
(Mouse)
protein kinase C signalling
Notch signalling pathway
positive regulation of protein kinase A signalling
vascular endothelial growth factor signalling pathway
positive regulation of MAPK cascade
Wnt signalling pathway
cerebral cortex GABAergic interneuron differentiation
synaptic transmission GABAergic
GABAergic neuron differentiation
midbrain development
GeneRatio
p.adjust
B
Number of inferred interaction
1605
2047
PAX6+/+
PAX6-/-
C
Interaction strength
0.276
0.089
PAX6+/+
PAX6-/-
D
PTN
VISFATIN
MK
BMP
ncWNT
IGF
PDGF
WNT
PAX6+/+
PAX6-/-
Interaction strength
E
RGP1
-log10(Padj)
log2(fold change)
C11orf96
DLX5
DLX6-AS1
DLX6
LINC01965
NKAIN3
NEUROD6
DLX2
GAD2
SLC32A1
SP9
PPP2R2B
CA5B
POTEI
AC069277.1
AC107398.3
PTCH1
TNR
GSX2
JAG1
NTRK2
OLIG1
F
RGP2
-log10(Padj)
log2(fold change)
AC069277.1
C11orf96
LINC01563
HSD17B11
PDZRN4
TLN2
GJA1
DLX2
SOX1-OT
DLX5
CNTN3
PREX2
GADD45G
FGD3
STOX1
NOS1AP
GAD1
GSX2
SP9
PLCE1
CCDC181
DLL1
AL139246.5
DLX6
FBN2
RHOJ
LINC01315
RGS16
HTR2A
MDM1
PEG10
INSM1
PDZRN3
ST8SIA5
FAI3
TMEM108
CHIC2
RND3
SLITRK1
DLK1
GAD2
BEST3
PDE4B